# General approach to spatiotemporal modulational instability processes

P. Béjot, Bertrand Kibler, E. Hertz, B. Lavorel, O. Faucher

▶ **To cite this version:**

P. Béjot, Bertrand Kibler, E. Hertz, B. Lavorel, O. Faucher. General approach to spatiotemporal modulational instability processes. Physical Review A : Atomic, molecular, and optical physics [1990-2015], 2011, 83, pp.013830. 10.1103/PhysRevA.83.013830 . hal-00576493

**HAL Id: hal-00576493**
**https://hal.science/hal-00576493**

Submitted on 14 Mar 2011

**HAL** is a multi-disciplinary open access archive for the deposit and dissemination of scientific research documents, whether they are published or not. The documents may come from teaching and research institutions in France or abroad, or from public or private research centers.

L'archive ouverte pluridisciplinaire **HAL**, est destinée au dépôt et à la diffusion de documents scientifiques de niveau recherche, publiés ou non, émanant des établissements d'enseignement et de recherche français ou étrangers, des laboratoires publics ou privés.

# General approach of spatiotemporal modulational instability processes

P. Béjot*, B. Kibler, E. Hertz, B. Lavorel, and O. Faucher
*Laboratoire Interdisciplinaire Carnot de Bourgogne,*
*UMR 5209 CNRS-Université de Bourgogne, BP 47870, 21078 Dijon Cedex, France**

In this paper, we derive the general exact solution of the modulation instability gain. The solution described here is valid for 1D, 2D, and 3D cases considering any temporal response function of the medium and with possible higher order Kerr nonlinearities. In particular, we show that the gain induced by modulation instability is initial conditions dependent while the usual calculations do not lead to such a dependence. Applications for current and high interest nonlinear propagation problems, such as 1D optical fiber propagation with delayed Raman response and 2D filamentation in gases, are investigated in details. More specifically, we demonstrate that the new 2D model of filamentation based on the balance between higher order Kerr terms leads to a new modulation instability window. The impact of both self-steepening and space-time defocusing effects is also highlighted. Finally, we discuss the influence of the finite time response of the different order electronic Kerr effects on the growth of the expected modulation instability bands.

PACS numbers: 42.65.Ky, 42.65.Sf, 42.81.Dp

## INTRODUCTION

From the 1960s till today, the modulation instability (MI) process has still remained the subject of numerous experimental and numerical studies in transparent materials [1–6]. When a quasi-continuous wave propagates through a nonlinear medium, it can experience, in appropriate phase-matching conditions, spatiotemporal instabilities that manifest themselves by the exponential growth of weak perturbations. More specifically, MI results from the interplay between linear effects, such as group velocity dispersion (GVD) or diffraction, and the Kerr induced nonlinearity. For instance, in optical waveguides, if the focusing (defocusing) nonlinear medium exhibits anomalous (normal) dispersion at the pump frequency $\omega_0$, because processes such as $\omega_0 + \omega_0 \rightarrow (\omega_0 + \omega) + (\omega_0 - \omega)$ can be nonlinearly phase matched, spectral bands spontaneously grow symmetrically with respect to the input wave frequency even in absence of any seed. However, both higher order dispersion and birefringence characteristics can strongly impact on the existence of new windows of scalar and vectorial MI effects [7, 8]. Similarly, MI can also appear in the spatial domain due to the balance between diffraction and Kerr effect. For instance, it has been shown that multifilamentation [10], *i.e.*, the splitting of an ultrashort ultra high power laser into several distinct structures is a direct manifestation of spatial MI. On the other hand, recent experiments have been able to determine the higher nonlinear refractive indices of gases such as argon, nitrogen, or oxygen [11]. These higher nonlinear indices manifest themselves at high intensity by the cancelation and even a sign reversal of the global nonlinear refractive index of the considered gases. These measurements are of particular importance for the understanding of pulse propagation dynamics since it has been demonstrated that, in some conditions, these indices are responsible for the collapse saturation during the filamentation process [12]. The scope of this paper is then twofold. In the first section, we theoretically study the stability of the nonlinear Schrödinger equation and derive the exact solution for MI. This solution is valid for 1D, 2D, and 3D propagation cases and is established with potential higher order Kerr terms and non-instantaneous temporal responses. The master equation derived here can hence describe any situation of scalar MI. To the best of our knowledge, it is the first time that such an exact solution is derived. Moreover, conversely to usual derivation of MI gain, we show that the gain bands are strongly dependent on the initial noise conditions. In the second section, we apply this new analytical basis to investigate in details the MI process for different configurations and materials. First, according to the recent measurements of higher order Kerr terms of some gases, we demonstrate the existence of a new 2D MI regime directly induced by these new nonlinear indices. Indeed, on-axis MI can occur in the normal dispersion regime when the global nonlinear refractive index becomes negative at very high intensities. Moreover, we analyze how the self-steepening and space-time defocusing terms modify the MI bands. Secondly, we show that the master equation gives also the exact solution of MI in optical fibers when delayed Raman effect is taken into account. In particular, we predict possible complex configurations of MI gain bands using the widely used waveguide category of photonic crystal fibers. Finally, we study the influence of the electronic finite time response on the MI. In particular, we demonstrate that the time response of the Kerr induced nonlinear index has to be relevantly evaluated in order to accurately describe the MI bands growth.

* pierre.bejot@u-bourgogne.fr

## I. MODULATIONAL INSTABILITY ANALYSIS

In this section, we consider a linearly polarized (along a vector $\mathbf{u}$) electric field propagating in a transparent centro-symetric medium. The electric field can be written as

$$\mathbf{E}(\overrightarrow{r},z,t)=(\varepsilon(\overrightarrow{r},z,t)e^{ik_0z-i\omega_0t}+\text{c.c.})\mathbf{u} \quad (1)$$

where c.c. denotes complex conjugation, $\varepsilon$ is the slowly varying envelope, $\overrightarrow{r}$ is the transverse direction, and $k_0$ is the wavevector at the associated pulsation $\omega_0$.

In the frame propagating at the pump frequency group velocity $v_g=1/k^{(1)}$ and neglecting harmonic generation, $\varepsilon$ verifies

$$\partial_z\varepsilon=\frac{i}{2k_0}T^{-1}\triangle_\perp\varepsilon+i\sum_{n\geq2}\frac{k^{(n)}}{n!}(i\partial_t)^n\varepsilon+iTk_0\Delta n\varepsilon \quad (2)$$

where $k^{(n)}=\frac{\partial^n k}{\partial\omega^n}|_{\omega_0}$ is the n$^{th}$-order dispersion coefficient of the medium evaluated at $\omega_0$ and $\Delta n$ is the nonlinear refractive index. $\triangle_\perp=\frac{\partial^2}{\partial x^2}+\frac{\partial^2}{\partial y^2}$ in 3D or $\triangle_\perp=\frac{\partial^2}{\partial r^2}+\frac{1}{r}\frac{\partial}{\partial r}$ in 2D denotes the transverse Laplacian. Assuming that the medium is transparent, $\Delta n$ can be written as $\Delta n=\sum_{j\geq1}n_{2j}R_{2j}(t)\star|\varepsilon|^{2j}$ where $\star$ accounts for convolution [13]. Depending on the considered medium, one can consider only $n_2$ (for instance, for propagation in fiber) or a full development up to $n_{10}$ (as shown in [12]). $R_{2j}(t)$ account for the $(2j+1)^{th}$ order temporal response function of the medium which are all real and verify $\int_{-\infty}^{\infty}R_{2j}(t)dt=1$ and $R_{2j}(t<0)=0$. $R_2(t)$ can take into account both electronic induced nonlinear response (generally admitted as instantaneous) and vibrational or rotational response. For instance, for silica fiber propagation problems, one generally takes $R_2(t)=(1-f_r)\delta(t)+f_rH(t)$ with $H(t)=f_ah_a(t)+f_bh_b(t)$, where $\delta$ is the Dirac function, $h_a=\tau_1(\tau_1^{-2}+\tau_2^{-2})e^{-t/\tau_2}\sin(t/\tau_1)$, $h_b=\frac{2\tau_b-t}{\tau_b}e^{-t/\tau_b}$, $f_r=0.18$, $f_a=0.79$, $f_b=0.21$, $\tau_1=12.2$ fs, $\tau_2=32$ fs, $\tau_b=96$ fs and $n_{2j}$ $(j>1)$=0 [14]. In air propagation problem, one takes $R_2(t)=(1-f_r)\delta(t)+f_rH(t)$ where $H(t)=\tau_1(\tau_1^{-2}+\tau_2^{-2})e^{-t/\tau_2}\sin(t/\tau_1)$, $f_r=0.5$, $\tau_1=62.5$ fs, $\tau_2=70$ fs with the higher order nonlinear indices $n_{2j}$ measured recently in [11]. In both cases, the electronic nonlinear response is considered as instantaneous. Finally, $T=1+\frac{ik^{(1)}}{k_0}\partial_t$ (resp., $T^{-1}=1-\frac{ik^{(1)}}{k_0}\partial_t$) accounts for self-steepening (resp., for space-time defocusing). Equation 2 allows to describe the propagation of electric field up to the single-cycle limit [15].

The steady state solution (*i.e.*, considering a monochromatic plane wave) of Eq. 2 can be expressed as

$$\varepsilon(z)=\sqrt{I_0}e^{ik_0D_nz}, \quad (3)$$

with $D_n=\sum_{j\geq1}n_{2j}I_0^j$ and $I_0$ the incident intensity.

The stability of the continuous-wave steady state solution of Eq. 2 is examined by studying the evolution of the system in presence of a small complex perturbation *a(r, t)*

$$\varepsilon(z)=\left(\sqrt{I_0}+a(r,t)\right)e^{ik_0D_nz}, \quad (4)$$

with $|a(r,t)|^2<<I_0$. Substituting Eq. 4 into Eq. 2 and linearizing, we find the equation describing the evolution of $a(r,t)$

$$\begin{aligned}\partial_za(r,t)=&T^{-1}\frac{i}{2k_0}\triangle_\perp a(r,t)+i\left(\sum_{n\geq2}\frac{k^{(n)}}{n!}(i\partial_t)^n\right)a(r,t)\\&+iTk_0I_0n_{2_{\text{eff}}}(t)\star\left(a(r,t)+a^*(r,t)\right),\end{aligned}$$

where

$$n_{2_{\text{eff}}}(t)=\sum_{j\geq1}jR_{2j}(t)n_{2j}I_0^{j-1}. \quad (5)$$

If one considers a cylindrical symmetry around the propagation axis and considering that $a(r,t)=\mathcal{H}\left(\int_{-\infty}^{\infty}\widetilde{a}(k_\perp,\omega)e^{-i\omega t}d\omega\right)$, where $\mathcal{H}$ is the Hankel transform defined as $\mathcal{H}(f)(r)=\int_0^\infty k_\perp J_0(k_\perp r)f(k_\perp)dk_\perp$ with $J_0$ the zeroth order Bessel function, one obtains the propagation equation for $\widetilde{a}(k_\perp,\omega)$

$$\begin{aligned}\partial_z\widetilde{a}(k_\perp,\omega)=&-i\left(\frac{k_\perp^2}{2k_0}(1-\frac{k^{(1)}}{k_0}\omega)-\sum_{n\geq2}\frac{k^{(n)}}{n!}\omega^n\right)\widetilde{a}(k_\perp,\omega)\\&+ik_0(1+\frac{k^{(1)}}{k_0}\omega)I_0n_{2_{\text{eff}}}(\omega)\left(\widetilde{a}(k_\perp,\omega)+\widetilde{a}^*(-k_\perp,-\omega)\right),\end{aligned} \quad (6)$$

where $n_{2_{\text{eff}}}(\omega)=\int_{-\infty}^{\infty}n_{2_{\text{eff}}}(t)e^{i\omega t}dt$.

Writing the equation propagation for $\widetilde{a}^*(-k_\perp,-\omega)$, using the fact that $n_{2_{\text{eff}}}(\omega)=n_{2_{\text{eff}}}^*(-\omega)$ (since all $R_{2j}(t)$ are real) and defining $u=\widetilde{a}(k_\perp,\omega)+\widetilde{a}^*(-k_\perp,-\omega)$ and $v=\widetilde{a}(k_\perp,\omega)-\widetilde{a}^*(-k_\perp,-\omega)$, $u$ and $v$ then satisfy the following partial differential equations system

$$\begin{aligned}\frac{\partial u}{\partial z}&=i(D_-u+(D_++S)v)\\\frac{\partial v}{\partial z}&=i\left[(D_++N)u+D_-v\right],\end{aligned} \quad (7)$$

where

$$\begin{aligned}D_+&=-\frac{k_\perp^2}{2k_0}+\sum_{n\geq1}\frac{k^{(2n)}}{(2n)!}\omega^{2n},\\N&=2k_0I_0n_{2_{\text{eff}}}(\omega),\\D_-&=\frac{k_\perp^2k^{(1)}}{2k_0^2}\omega+\sum_{n\geq1}\frac{k^{(2n+1)}}{(2n+1)!}\omega^{2n+1},\\S&=2k^{(1)}\omega I_0n_{2_{\text{eff}}}.\end{aligned}$$

Defining $K = \sqrt{-D_+(D_+ + N) - \frac{S^2}{4}}$ and $\Phi(z) = (D_- + S/2)z$, the two solutions of Eq. 7 are

$$u(z) = \frac{e^{i\Phi(z)}}{2} \times \left( u_0 \cosh(Kz) + i\frac{D_+ v_0 + \frac{S}{2}u_0}{K} \sinh(Kz) \right)$$
$$v(z) = \frac{e^{i\Phi(z)}}{2} \times \left( v_0 \cosh(Kz) + i\frac{(D_+ + N)u_0 - \frac{S}{2}v_0}{K} \sinh(Kz) \right),$$

where $u_0(k_\perp, \omega) = u(k_\perp, \omega, z = 0)$ and $v_0(k_\perp, \omega) = v(k_\perp, \omega, z = 0)$. Finally, the evolution of the perturbation $\widetilde{a}(k_\perp, \omega)$ can be expressed as

$$\widetilde{a}(k_\perp, \omega) = e^{i\Phi(z)} \left( \widetilde{a}_0 \cosh(Kz) + i\frac{\widetilde{A_0}}{K} \sinh(Kz) \right), \tag{8}$$

where $\widetilde{A_0} = (D_+\widetilde{a}_0 + \frac{N}{2}(\widetilde{a}_0 + \widetilde{a}_0{}^\sharp) + \frac{S}{2}\widetilde{a}_0{}^\sharp$, with $\widetilde{a}_0 = \widetilde{a}(k_\perp, \omega, z = 0)$ and $\widetilde{a}_0{}^\sharp = \widetilde{a}^*(-k_\perp, -\omega, z = 0)$.

In the following numerical simulations, $\widetilde{a}_0$ is the initial noise spectrum calculated as $\widetilde{a}_0 = \mathcal{H}\left(\int_{-\infty}^{\infty} a(r, t, z = 0)e^{i\omega t}dt\right)$ while $\widetilde{a}_0{}^\sharp$ is calculated as $\widetilde{a}_0{}^\sharp = \mathcal{H}\left(\int_{-\infty}^{\infty} a^*(r, t, z = 0)e^{i\omega t}dt\right)$.

The evolution of the spatio-temporal noise is then govern by Eq. 8. In particular, MI occurs when $\mathcal{R}_e(K) > 0$, *i.e.*, when $D_+(D_+ + N) + \frac{S^2}{4} < 0$, roughly leading to an exponential growth of $a$. More precisely, MI occurs if $\frac{-N-\sqrt{N^2-S^2}}{2} < D_+ < \frac{-N+\sqrt{N^2-S^2}}{2}$. Equation 8 is a general solution of MI in any nonlinear medium which can present a delayed nonlinear response and higher order nonlinear Kerr terms. However, one has to emphasize that this equation can be extended to a 3D model by replacing $k_\perp^2$ by $k_x^2 + k_y^2$ and considering a 2D spatial Fourier transform instead of an Hankel transform. Moreover, the 1D case (*i.e.*, for fiber propagation issues) is obtained by setting $k_\perp = 0$. To the best of our knowledge, it is the first time that the *exact* solution of the evolution of the noise is derived. One generally uses an ansatz function for $a$ [8, 19–23]. Using such a method does not allow to retrieve the *exact* solution for the evolution of $a$. Instead, one can only evaluate a gain (which *does not* intrinsically depend on the initial seeding). The fact that the growth is dependent on the initial noise could play a role in rogue wave generation [16]. Moreover, considering the initial conditions dependence of Eq. 8 at a fixed $\omega$, the maximal gain is dependent on the spatial gradient of both $\widetilde{a}_0$ and $\widetilde{a}_0{}^\sharp$. Consequently, it explains why multifilamentation occurs in the region of strong noise gradient. Since we have neglected the nonlinear terms with respect to $a$, the only limit of validity of this model is potential cascading phenomena which can occur when $|a|^2$ becomes non-negligible.

## II. RESULTS AND DISCUSSION

### A. 2D analysis

In this section, we consider the propagation in Argon of a cylindrical pump beam in order to investigate the impact of its higher order Kerr coefficients which have been recently measured up to $n_{10}$ [11]. Moreover, we assume here that all the nonlinear responses are instantaneous, *i.e.*, $R_{2j}(t) = \delta(t)\ \forall j$. Figure 1 shows the comparison between the integration of Eq. 2 and the results obtained from Eq. 8 for two different regimes in argon at atmospheric pressure and in a normal dispersion regime. As demonstrated in [12], Eq. 2 can accurately describe the propagation of filaments providing that the plasma contribution stays negligible. The numerical simulations were performed by starting from a CW pump with a superimposed small noise (with a random spectral phase added to each frequency bin) as a seed for the MI. Since in real experiments, the perturbations have their maximum intensity at the laser central frequency, in the frequency domain, and at the center of the pulse, in the spatial domain, we have also checked that using a noise with an amplitude presenting a gaussian distribution centered on the pump frequency in both spectral and spatial domain does not affect qualitatively the MI bands. We clearly note the excellent quantitative agreement between analytical and numerical results, thus confirming the validity of our calculations. It is worth mentioning that calculations using an ansatz would only allow to retrieve the envelope of the gain but not its fine structure.

Figure 1(a) (resp., (b)) displays the analytical (resp., the numerical) MI gain bands for a 20 TW.cm$^{-2}$ pump propagating trough 1 m of Argon at atmospheric pressure. At low intensities ($n_{2_{\text{eff}}} > 0$), the gain displays a X pattern in the $(k_\perp, \omega)$ space. Neglecting higher order dispersion coefficients, four-wave mixing (FWM) processes $\omega_0 + \omega_0 \rightarrow (\omega_0 + \omega) + (\omega_0 - \omega)$ are phase matched if the condition $\frac{N-\sqrt{N^2-S^2}}{2} \leq \frac{k_\perp^2}{2k_0} - k^{(2)}\omega^2 \leq \frac{N+\sqrt{N^2-S^2}}{2}$ is respected. At the pump frequency ($\omega = 0$) and considering the temporal response of the medium as instantaneous, instabilities are maximal for $k_{\perp_{max}}^2 = 2k_0^2 I_0 n_{2_{\text{eff}}}$. This instability can then lead to the pulse break-up and consequently to multi-filamentation. Moreover, one can associate to this instability a power $P = \pi I_0 / k_{\perp_{max}}^2 = \lambda_0^2/(8\pi n_{2_{\text{eff}}})$ which corresponds to the widely-studied critical power. Neglecting the higher order Kerr terms, if a pulse carries a power above $P$, then it will lead to a self-similar blowup singularity of Eq. 2 and to the pulse collapse [1].

For other frequencies, instabilities are maximal for $k_{\perp_{\max}}^2 = 2k_0\left(\sum_{n\geq 1} \frac{k^{(2n)}}{(2n)!}\omega^{2n} + k_0 I_0 n_{2_{\text{eff}}}\right)$. Figure 2

compares the emission angle $\theta(\omega)$=$k_{\perp_{max}}/k(\omega)$ obtained with our calculations with those experimentally measured in the visible [24] and in the infrared [25]. Even if MI calculations are intrinsically done with a continuous plane wave with an infinite spatial extension (which does not correspond to filamentation of ultrashort pulses), MI calculations accurately reproduce the conical emission induced during the filamentation. The good agreement between our calculations and the angles measured experimentally consequently confirms that conical emission is indeed generated by off-axis four waves mixing (4WM) during filamentation when $n_{2_{eff}} > 0$.

The situation significantly changes at higher intensity when $n_{2_{eff}} < 0$. In particular, the X pattern completely disappears but a new mechanism of MI still occurs. As stated beforehand, MI occurs as soon as the condition $D_+(D_+ + N) + \frac{S^2}{4} > 0$ is respected. This condition is equivalent to

$$n_- < n_{2_{eff}}(\omega) I_0 < n_+, \tag{9}$$

with

$$n_- = -\frac{k_0 D_+ \left(2 - \frac{k^{(1)^2}\omega^2}{2k_0^2}\right)}{k^{(1)^2}\omega^2},$$
$$n_+ = -\frac{D_+}{2k_0}.$$

More particularly, Fig. 3 displays the frequency range where on-axis ($k_\perp$=0) MI is possible. When $I_0$ lies in the range 23.5-31.9 TW.cm$^{-2}$, on-axis MI occurs. At higher intensity, $\forall$ ($k_\perp$, $\omega$), $n_{2_{eff}} I_0 < n_-$, meaning that no phase matching and consequently, no MI can occur.

As a result, one can distinguish two cases. At moderate intensities (30 TW.cm$^{-2}$, Figs. 1(c,d)) such that $n_- < n_{2_{eff}} I_0 < n_+$, strong on-axis MI is observed. For higher input intensities (40 TW.cm$^{-2}$, Figs.1(e-f)), the gain drastically decreases since the phase matching condition is not fulfilled anymore.

One has to note that Théberge et al. [25] have observed on-axis infrared emission which cannot be explained by off-axis 4WM processes. The MI calculations show that such type of on-axis emission appears as soon as $n_{2_{eff}} < 0$.

One should emphasize that the general solution can be used to enhance or reduce the gain at specific frequencies by adjusting the phase and amplitude of the initial seeding. Figure 4 displays the MI gain bands for a pump intensity of 30 TW.cm$^{-2}$ when $\widetilde{a_0}$ and $\widetilde{a_0}^\sharp$ are in phase (red) and out of phase (blue). By adjusting their relative phase, the gain can be enhanced or reduced, the latter being maximal (resp., minimal) when $\widetilde{a_0}$ and $\widetilde{a_0}^\sharp$ are in phase (resp., out of phase).

We have shown above that the higher order Kerr terms lead to on-axis MI in the normal dispersion regime. In this paragraph, we study the influence of self-steepening (SS) and space-time defocusing (STD) on the MI band

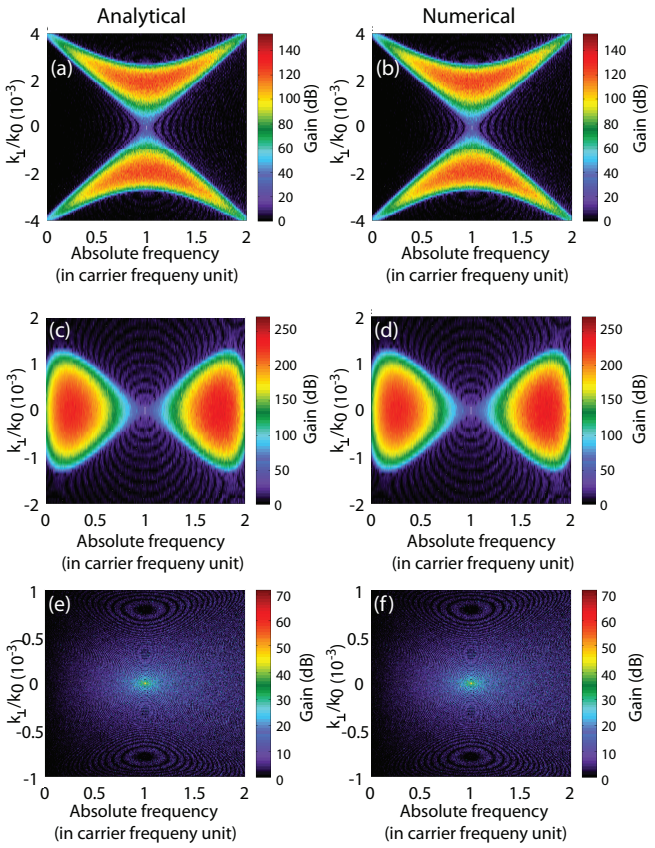


Figure 1. Color Online. Analytical (a) (resp., (c) and (e)) and numerical (b) (resp., (d) and (f)) MI gain (dB) after propagation of a 20 TW.cm$^{-2}$ (resp., 30 TW.cm$^{-2}$ and 40 TW.cm$^{-2}$) pump trough 1 m in argon when taking into account both self-steepening and space-time defocusing.

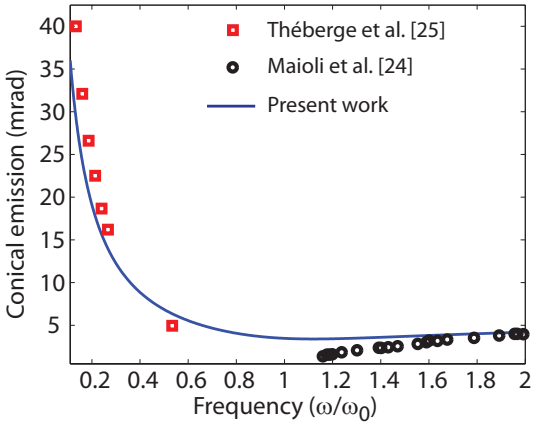


Figure 2. Color Online. Comparison between experimental measurements of conical emission in the visible (black circle) and in the infrared (red square) with MI calculations (blue line).

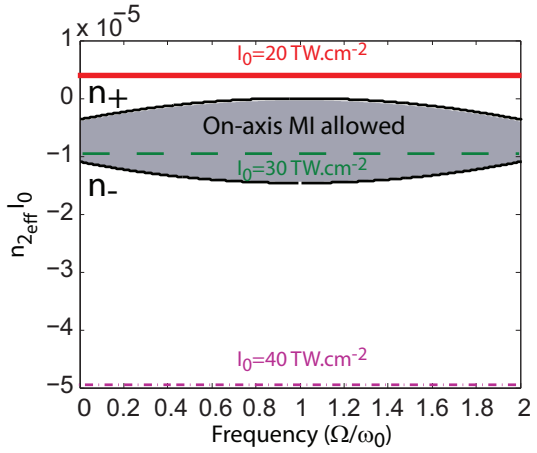


Figure 3. Color Online. Diagram displaying the spectral region where on-axis MI occurs (grey region) and lying between $n_+$ and $n_-$ (black lines). The lines displayed $n_{2_{\rm eff}}$ $I_0$ with $I_0$=20 TW.cm$^{-2}$ (red solid), 30 TW.cm$^{-2}$ (dashed green), and 40 TW.cm$^{-2}$ (dotted-dash violet) assuming the Kerr response as instantaneous, *i.e.*, $n_{2_{\rm eff}}(\omega)$=$n_{2_{\rm eff}}$ $\forall$ $\omega$.

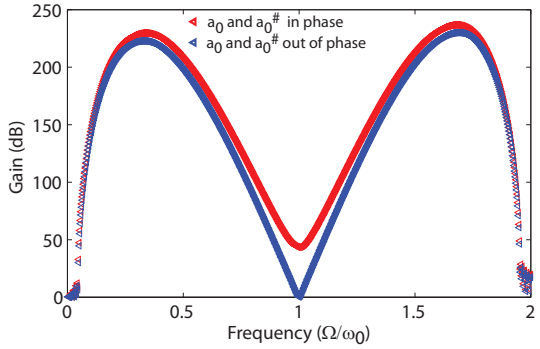


Figure 4. Color Online. Gain bands through 1 m argon for a pump of 30 TW.cm$^{-2}$ when $\widetilde{a_0}$ and $\widetilde{a_0}^\sharp$ are in phase (red) and out of phase (blue).

growth. The effect of these terms has already been discussed in [26]. However, our general expression obtained in section I allows us to better capture the MI dynamics. To perform this study, we have removed the contributions of these two terms (by setting $k^{(1)}=0$) from the analytical and the numerical calculations and we have repeated the same calculations than in the previous section. In Figs. 5(a-b), the intensity of the pump is 20 TW.cm$^{-2}$ so that $n_{2_{\rm eff}}>0$. In that condition, neglecting both SS and STD does not lead to significant change of the MI bands. Only a slight deviation of the emission pattern can be noticed at frequencies far from the frequency pump. In the intermediate regime shown in Figs. 5(c-d), both shape and value of the gain change. In particular, neglecting SS and STD leads to a dramatic over-estimation of the MI. This is due to the fact that the coupling between the pump and the MI bands is over-estimated if one neglects

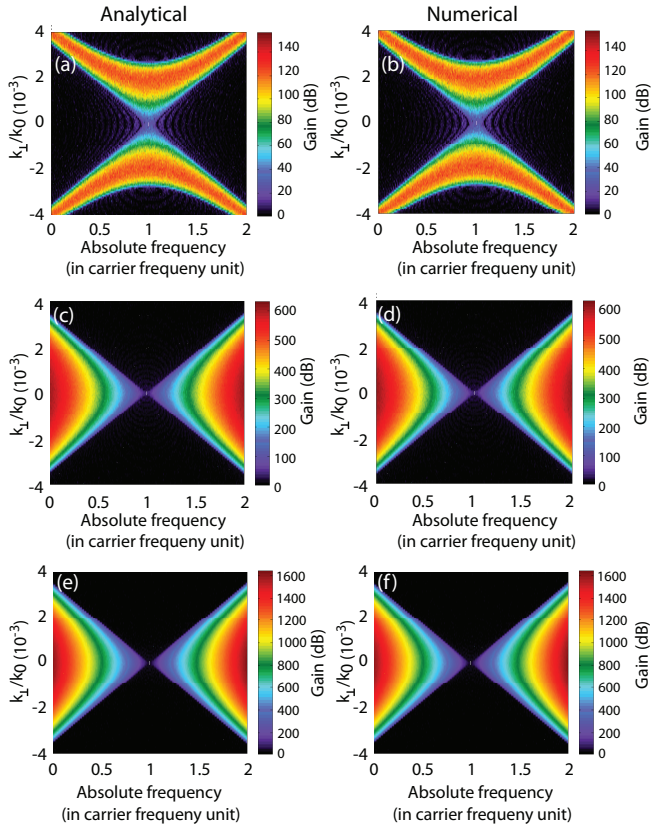


Figure 5. Color Online. Comparison between numerical and analytical calculations of the gain (dB) in the $(k_\perp,\omega)$ space when neglecting both self-steepening and space-time defocusing. (a,b) Gain induced by a 20 TW.cm$^{-2}$ pump ($n_{2_{\rm eff}}>0$), (c,d) gain induced by a 30 TW.cm$^{-2}$ pump ($n_{2_{\rm eff}}<0$) and (e,f) gain induced by a 40 TW.cm$^{-2}$ pump ($n_{2_{\rm eff}}<<0$) after 1 m propagation.

SS and STD far from the frequency pump. Hence, without SS and STD, the maximal gain is obtained at $\omega$=0 and $\omega$=2$\omega_0$ while the full calculation gives the frequencies of maximal gain are $\omega$=0.3 $\omega_0$ and $\omega$=1.7 $\omega_0$ (see Fig. 4). At higher intensities, Figs. 5(e,f), the MI gain bands are dramatically over-estimated.

It results from Figs. 5(e,f) that neglecting both SS and STD suppresses the regime where MI is annihilated (high intensity regime). When neglecting both SS and STD, the condition which has to be respected for the MI to occur is reduced to

$$n_{2_{\rm eff}}(\omega)I_0 < n_+. \qquad (10)$$

When the intensity increases, this condition is always respected which leads to MI as shown in Fig. 6.

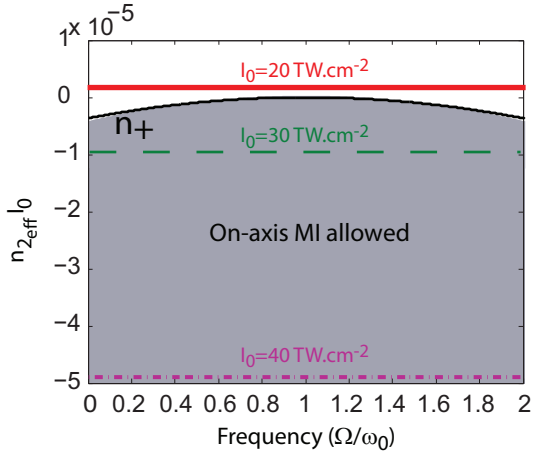


Figure 6. Color Online. Diagram displaying the spectral region where on-axis MI occurs (grey region) when neglecting both SS and STD. This region is below $n_+$ (black line). The lines displayed $n_{2_{eff}}$ $I_0$ with $I_0$=20 TW.cm$^{-2}$ (red solid), 30 TW.cm$^{-2}$ (dashed green), and 40 TW.cm$^{-2}$ (dotted-dash violet) assuming the Kerr response as instantaneous, *i.e.*, $n_{2_{eff}}(\omega)$=$n_{2_{eff}}$ $\forall$ $\omega$.

### B. 1D analysis in presence of Raman induced delayed nonlinear response

In order to underline the generality of the solution derived in section 1, we calculated analytical and numerical solutions of the MI gain induced in a single mode fiber (SMF) in presence of vibrational Raman nonlinearity. We considered the propagation of a 1550 nm 5 GW.cm$^{-2}$ continuous wave in a 15 cm-long standard SMF (anomalous dispersion $k^{(2)}$ = −2.1 10$^{-26}$ s$^2$.m$^{-1}$ and positive nonlinear index $n_2$ = 2.6 10$^{-20}$ m$^2$.W$^{-1}$) when vibrational Raman effect is taken into account. Figure 7(a) displays both analytical and numerical MI-Raman gain bands. Since the general solution here takes into account the contributions of both real and imaginary parts of the Raman effect, the global gain is no more symmetric with respect to the pump frequency, with an amplification (resp., absorption) at longer (resp., shorter) wavelengths. We confirm again the excellent quantitative agreement between analytical and numerical results by showing in Fig.7(b) that the relative error is less than 1%. The slight discrepancies are mainly due to the finite propagation step used during the split-step Fourier numerical simulation. The combined action of parametric and Raman effects was already discussed in the early work of Shen and Bloembergen [17] and later the resulting global (parametric-raman) gain was widely investigated in the context of optical fibers [18, 19, 21, 22]. With our general solution, the results obtained in these works can be retrieved only by calculating the parameter $K$. However, the gain evaluated with the help of an ansatz function (as shown in Fig. 7(a)) is only a rough estimation of the real gain, in particular around the pump frequency. Moreover, calculating $K$ cannot describe the asymmetry induced by the imaginary part of the Raman response function. When the MI gain bands do not overlap the Raman bands, positive gain is expected in the anti-Stokes band when simply evaluating $K$, while this part of the spectrum actually undergoes losses as it can be noticed in Fig. 7(a).

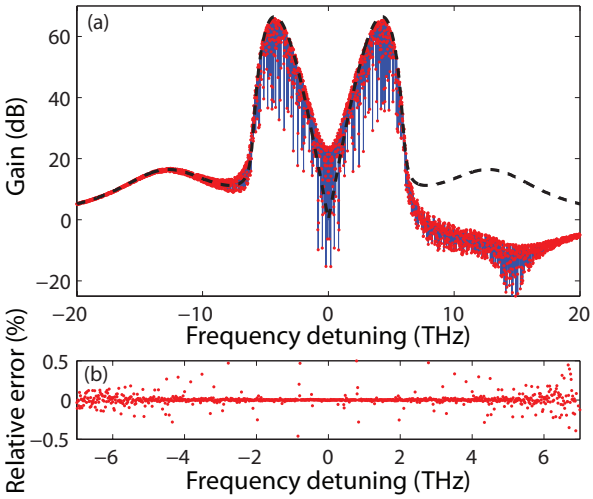


Figure 7. Color Online. (a) Analytical (red dots) and numerical (solid blue line) MI gain bands calculated after 15 cm propagation in a SMF fiber with a pump of 5 GW.cm$^{-2}$ in presence of a delayed Raman nonlinearity. The black dashed line represents the gain calculated using an ansatz function. (b) Relative error between numerical and analytical calculations.

Nowadays, fiber dispersion properties can be engineered to a very high degree, thus allowing phase-matching induced by higher order dispersion for ultra-broadband wavelength conversion [27]. For instance, the fourth-order dispersion can induce additional scalar MI bands in the normal dispersion regime [7]. It has been shown that in presence of negative fourth order dispersion near zero dispersion frequency, MI bands can grow up even by pumping in the normal dispersion regime. Consequently, by pumping in the anomalous dispersion regime, it is then possible to observe two pairs of MI sidebands [23]. We consider here this possible complex configuration of the MI process using the waveguide category of photonic crystal fibers (PCF). Figure 8 compares the analytical and numerical gain bands obtained by pumping a photonic crystal fiber which exhibits a low anomalous dispersion between its two zero dispersion wavelengths. Both linear and nonlinear fiber properties can be found in [28]. We used a 2.6 GW.cm$^{-2}$ pump intensity at 1064 nm and a fiber length of 1 m. It clearly appears that Eq. 8 is also able to perfectly retrieve the two pairs of MI sidebands induced by second and fourth order dispersion terms. Besides the impact of higher order dispersion on the phase matching, our solution describes the asymmetrical shape of MI induced by the Raman gain. Indeed,

we have adjusted here the input wave intensity so that the first standard MI sidebands are superposed to the silica Raman gain band (0-30 THz). Consequently, we retrieve again that the global MI-Raman gain is no more symmetric with respect to the pump frequency. As previously, the standard gain evaluation can give a rough estimation of the real gain in specific conditions.

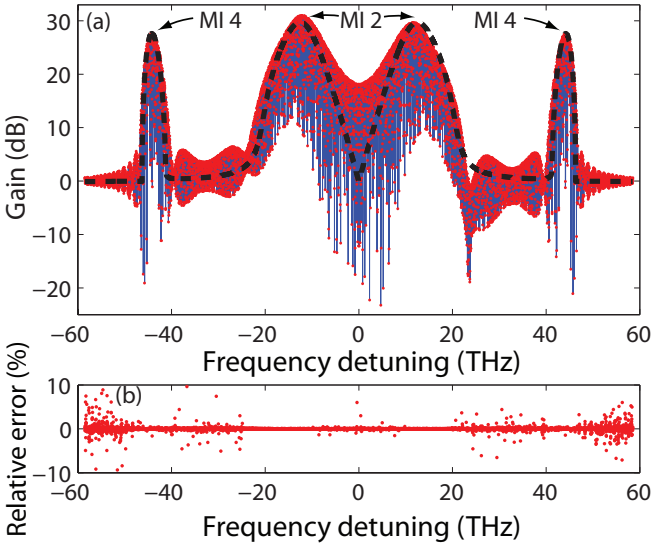


Figure 8. Color Online. (a) Numerical (blue line) and analytical (red dots) MI gain bands obtained in 1m-long PCF with two zero dispersion frequencies in presence of a delayed Raman nonlinearity. The black dashed line represents the gain calculated using an ansatz function. (b) Relative error between analytical and numerical calculations.

### C. Impact of Kerr electronic time response on the MI bands growth

In this section, we underline the impact of the time response of the different higher order nonlinear Kerr terms on the induced MI. A recent work has highlighted the influence of a finite nonlinear response time [29] on the spatio-temporal MI growth but by using the usual simplified approach. Conversely, our method gives the exact solution even in presence of a delayed nonlinear response without any approximation. Since the systematic study of any situation of MI is out of the scope of the present paper, we have limited our work to 1D MI gain in argon (as for instance relevant in the frame of hollow core fiber propagation [30, 31]) with non purely instantaneous nonlinear responses. Since no accurate information about the time response of the higher order nonlinearities are so far available, we used the same expression for all nonlinearities (*i.e.*, the Debye type relaxation model). We write $\forall j,\ R_{2j}(t) = \frac{1}{\tau}e^{-t/\tau}$ for $t > 0$ and $R_{2j}(t) = 0$ for $t < 0$, although the different terms exhibit *a priori* distinct temporal behaviors. We used three distinct values of $\tau$ (0, 0.5 fs, and 2 fs) for pump intensities of 20, 30 and, 40 TW.cm$^{-2}$ which correspond to the three regimes observed when the Kerr effect is supposed to be instantaneous. Figure 9 displays the MI bands calculated after a 1 m propagation through 1 bar of argon with the same initial noise. In the low intensity regime (Fig.9(a)), while MI is not allowed for $\tau$=0, on-axis MI is allowed when increasing $\tau$. On the contrary, in the intermediate regime (Fig.9(b)), a reduction by twenty orders of magnitude of the generated MI bands is observed when increasing the time response. Finally, in the high intensity regime (Fig.9(c)), increasing the time response leads to MI while phase matching cannot be achieved if $\tau$=0. It appears that even for very small values, the Kerr electronic time response is crucial to accurately describe the efficiency of MI bands generation. In particular, we show that increasing the time response from 0 to 2 fs leads to a drastic change of the MI bands in all intensity regimes.

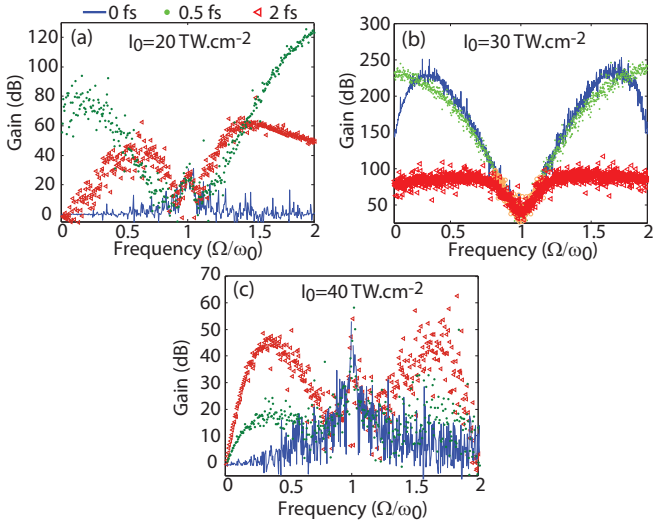


Figure 9. Color Online. On-axis gain bands after 1 m propagation through Argon with a pump of 20 TW.cm$^{-2}$ (a), 30 TW.cm$^{-2}$ (b), and 40 TW.cm$^{-2}$ (c) with different Kerr electronic time responses (0 fs (blue line), 0.5 fs (green dots), and 2 fs (red triangles)).

## III. CONCLUSION

In this paper, we have derived the general expression of modulation instability in presence of a continuous plane wave pump. The model, valid in 3D, 2D, and 1D, allows to evaluate the MI gain in presence of higher order Kerr terms and any retarded nonlinear response (including the Raman response). We have shown that, if the propagation of a pulse can be described by the equilibrium between the Kerr terms, then on-axis MI bands grow up as soon as the effective nonlinear index becomes negative. We have also highlighted the impact of self-steepening, space-time defocusing, and finite time non-

linear response on the MI band growth. Finally, in the frame of fiber propagation problem, we have shown that our analytical model perfectly describes the MI bands growth in presence of Raman effect and complex dispersive properties. Moreover, we foresee that comparable analytical solutions can be found for vectorial MI, *i.e.*, for propagation through birefringent medium.

## IV. ACKNOWLEDGMENT

We gratefully acknowledge K. Hammani, P. Morin, and G. Millot for very fruitful discussions. This work was supported by the ANR COMOC ANR-07-BLAN-0152-01 and FASTQUAST ITN Program of the seventh FP. B. Kibler acknowledges support from the French Agence Nationale de la Recherche project MANUREVA ANR-08-SYSC-019 and from the Conseil Régional de Bourgogne.

[1] V.I. Bespalov and V.I. Talanov, JETP Letter **3**, 307-310 (1966)
[2] T.B. Benjamin and J.E. Feir, J. Fluid Mech. **27**, 417-430 (1967)
[3] K. Tai, A. Hasegawa, and A. Tomita, Phys. Rev. Lett. **56**, 135-139 (1986)
[4] D. Kip, M. Soljacic, M. Segev, E. Eugenieva, D.N. Christodoulides, Science **290**, 495-498 (2000)
[5] V.E. Zakharov and L.A. Ostrovsky, Physica D **238**, 540-548 (2009)
[6] J.M. Dudley, G. Genty, F. Dias, B. Kibler, N. Akhmediev, Optics Express **17**, 21497-21508 (2009)
[7] S. Pitois and G. Millot, Optics Comm. **226**, 415-422 (2003)
[8] F. Biancalana and D.V. Skryabin, J. Opt. A **6**, 301-306 (2004)
[9] S. Tzortzakis, L. Bergé, A. Couairon, M. Franco,B. Prade, and A. Mysyrowicz, Phys. Rev. Lett. **86**, 5470-5473 (2001)
[10] F. Vidal and T.W. Johnston, Phys. Rev. Lett. **77** (7) 1282-1285 (1996)
[11] V. Loriot, E. Hertz, O. Faucher, and B. Lavorel, Opt. Express **17**, 13429 (2009); Erratum in Opt. Express **18** 3011 (2010)
[12] P. Béjot, J. Kasparian, S. Henin, V. Loriot, T. Vieillard, E. Hertz, O. Faucher, B. Lavorel, and J.-P. Wolf, Phys. Rev. Lett. **104**, 103903 (2010).
[13] J.-L. Oudar, J. Quant. Electron. **19**, 713-718 (1983)
[14] Q. Lin and G.P. Agrawal, Opt. Lett. **31**, 21 (2006)
[15] T. Brabec and F. Krausz, Phys. Rev. Lett. **78** 17 3282-3285 (1997)
[16] D. R. Solli, C. Ropers, P. Koonath, and B. Jalali, Nature **450**, 1054-1057 (2007)
[17] N. Bloembergen and Y. R. Shen, Phys. Rev. Lett. **12**, 504-507 (1964)
[18] M.J. Potasek, Opt. Lett. **12**, 921-923 (1987)
[19] S. Trillo and S. Wabnitz, J. Opt. Soc. Am. B **9**, 1061 (1992)
[20] J.E. Rothenberg, Phys. Rev. A **42**, 682 (1990)
[21] K.J. Blow and D. Wood, IEEE J. Quant. Electron **25**, 2665 (1989)
[22] E.A. Golovchenko and A.D. Pilipetskii, J. Opt. Soc. Am. B **11**, 92-101 (1994)
[23] F. Biancalana, D. V. Skryabin, and P. St. J. Russell, Phys. Rev. E **68**, 046603 (2003)
[24] P. Maioli, R. Salamé, N. Lascoux, E. Salmon, P. Béjot, J. Kasparian and J.-P. Wolf, Opt. Express **17**, 4726-4731 (2009)
[25] F. Théberge, M. Chateauneuf, V. Ross, P. Mathieu, and J. Dubois, Opt. Lett. **33**(21), 2515-2517 (2008)
[26] S. Wena, W. Hua, H. Guoa, and D. Fan, Optics Comm. **202** 339-346 (2002)
[27] P. St.J. Russell, J. Light. Technol. **24**, 4729-4749 (2006)
[28] B. Barviau, B. Kibler, A. Kudlinski, A. Mussot, G. Millot, and A. Picozzi, Opt. Express **17**, 7392-7406 (2009)
[29] L. Zhang, S. Wen, X. Fu, J. Deng, J. Zhang, and D. Fan, Opt. Comm. **283** 2251-2257 (2010)
[30] P. Béjot, B.E. Schmidt, J. Kasparian, J.-P. Wolf, and F. Legaré, Phys. Rev. A **81**, 063828 (2010)
[31] B.E. Schmidt, P. Béjot, M. Giguère, A.D. Shiner, C. Trallero-Herrero, E. Bisson, J. Kasparian, J.-P. Wolf, D.M. Villeneuve, J.-C. Kieffer, P.B. Corkum, and F. Légaré, Appl. Phys. Lett. **96**, 121109 (2010)